



Contents lists available at ScienceDirect

Chinese Chemical Letters

journal homepage: www.elsevier.com/locate/ccllet

sp² carbon conjugated covalent organic cage with efficient photocatalysis



Jiajia Li^{a,b}, Shan Shiang Hii^b, Xinyuan Zhu^b, Yanping Yang^{a,b,*}, Youfu Wang^{b,*}

^a School of Materials Science and Engineering, Shanghai University of Engineering Science, Shanghai 201620, China

^b School of Chemistry and Chemical Engineering, Shanghai Jiao Tong University, Shanghai 200240, China

ARTICLE INFO

Article history:

Received 20 January 2025

Revised 16 March 2025

Accepted 26 March 2025

Available online 27 March 2025

Keywords:

sp²c

Conjugation

Covalent organic cage

Knoevenagel condensation

Photocatalysis

ABSTRACT

The design and synthesis of fully conjugated covalent organic cages (cCOCs) featuring sp² carbon connections pose significant challenges due to the difficulties associated with forming stable C=C bonds. In this study, we present a novel anthracene-based cCOC linked by C=C bonds, synthesized directly through Knoevenagel condensation. Remarkably, this sp²c COC has shown exceptional performance as an n-type semiconductor, characterized by strong electronic delocalization, an optimized band structure, and extensive light absorption capabilities. It efficiently catalyzes the photodegradation of organic dyes and promotes the photoinduced aerobic oxidation of amines to imines. In comparison to imine-linked cCOCs with the same skeleton, the sp²c COC demonstrates distinct advantages as a next-generation photocatalyst, including enhanced chemical stability and superior photocatalytic performance. This research underscores the potential of Knoevenagel condensation in the development of innovative cCOCs, offering valuable insights for their applications in optoelectronic materials and catalysis.

© 2025 Published by Elsevier B.V. on behalf of Chinese Chemical Society and Institute of Materia Medica, Chinese Academy of Medical Sciences.

Conjugated covalent organic cages (cCOCs) are a class of three-dimensional (3D), carbon-rich nanoobjects formed by linking multiple conjugated units through conjugated covalent bonds, resulting in atomically precise structures with curved rigid skeletons and multiple interconnected windows [1]. Unlike traditional conjugated small molecules/polymers and nanocarbons, the curved and precise cCOCs confer relatively higher stability, tunable porosity, excellent solution processability, and remarkable optoelectronic properties, making them a highly sought-after emerging class of conjugated materials [2–4]. Despite significant progress in the past decade in developing cCOCs with functional skeletons through various bonding strategies and their applications in fields such as catalysis, biomedicine, and electronic devices, challenges remain. Complex synthesis protocols, limited availability of pre-organized building blocks, and low overall yields have made it a persistent challenge to construct cCOCs through simple and efficient universal synthesis strategies [1,2,4–8].

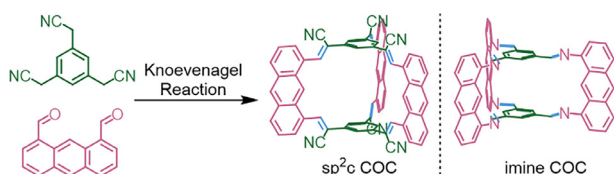
Dynamic covalent chemistry (DCC) is a well-established strategy for the effective construction of cCOCs [9]. In addition to the classical and widely applied Schiff base reactions to create C=N bonds linked cCOCs with complex structures and specific functionalities,

researchers have invested considerable effort into employing olefin and alkyne metathesis to construct cCOCs linked by more robust C=C and C≡C bonds. However, the intricate interactions involving thermodynamic stability and kinetic control make the mechanisms of dynamic metathesis unclear, complicating the precise construction of cCOCs with specific complex structures and functionalities [10,11]. In contrast, the base-catalyzed Knoevenagel condensation can directly yield high-purity cCOC crystals through a solvothermal process, with cCOCs linked by sp² C=C bonds demonstrating remarkable chemical stability under harsh conditions. In 2024, Prof. Yuan reported a series of sp²c COCs using the Knoevenagel condensation and highlighted the robust stability of sp² C=C bonds and validated the viability of this strategy [2]. This strategy has also been demonstrated its viability in the construction of sp²c covalent organic frameworks (COFs) [12–15]. Thus, by selecting specific photoactive monomers, cCOCs constructed using the Knoevenagel condensation could potentially exhibit excellent photocatalytic activity.

Herein, we designed and synthesized an olefin-linked cCOC, referred to as sp²c COC, enriched with anthracene groups via the Knoevenagel condensation of 1,8-dialdehyde-anthracene (An-2CHO) and 2,2',2''-(benzene-1,3,5-triyl)triacetonitrile (BTN) (Scheme 1). Owing to the photoreactivity of anthracene and the characteristics of the C=C bonds, the sp²c COC exhibited remarkable chemical stability, an optimal band structure, and strong light

* Corresponding authors.

E-mail addresses: yangyp0709@sues.edu.cn (Y. Yang), wfyfwn@sjtu.edu.cn (Y. Wang).



Scheme 1. Synthesis of sp^2c COCs through Knoevenagel reaction, as well as imine COC for comparison.

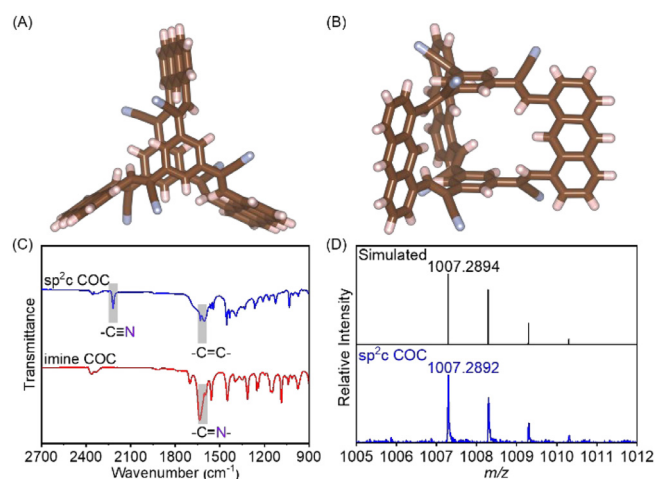


Fig. 1. Structural characterization of COCs. (A,B) Crystallographic images of sp^2c COC. (C) FT-IR spectra of sp^2c COC and imine COC. (D) HRMS analysis of sp^2c COC.

absorption capabilities. As a photoresponsive semiconductor, sp^2c COC demonstrated superior carrier conduction efficiency compared to imine COC due to its high degree of conjugation and electron delocalization. Beyond photocatalytic degradation of organic dyes, sp^2c COC can also effectively catalyze the direct transformation of amines to imines under light irradiation, showcasing impressive and sustained activity along with good reusability.

To synthesize sp^2c COC, BTN and An-2CHO were selected as the precursors. Given the low reversibility of the Knoevenagel condensation reaction, we conducted the reaction under solvothermal conditions. Specifically, An-2CHO (1.5 equiv.) were combined with BTN (1 equiv.) in *o*-DCB/MeOH (4:1 by volume) in the presence of Cs_2CO_3 , a base catalyst (Figs. S1-S6 in Supporting information). This mixture was sealed in a glass tube and heated at 85 °C for 12 h (Scheme S1 in Supporting information) [2,16]. The bulk sp^2c COC crystals were directly obtained using the solvothermal method and confirmed through crystallographic analysis (CCDC: 2375695). Single crystal X-ray diffraction (SCXRD) data indicated that the sp^2c COC crystals belong to the hexagonal system, with a space group of $P6_3/m$ and a unit cell volume of 3713.8(4) Å³. This highly symmetric lattice structure was commonly observed in mesoporous materials that exhibited excellent mechanical properties and catalytic activity. This suggested that sp^2c COC possessed intrinsic structural advantages, which inspired our interest in exploring its optoelectronic properties [17,18]. These colorless bulk crystals were identified as [2 + 3] cages with cavities, exhibiting a triangular prismatic shape (Figs. 1A and B, Fig. S7, and Table S1 in Supporting information). The high-resolution mass spectrum (HRMS) data further supported the [2 + 3] cage structure, showing a molecular weight of m/z 1007.2892 for the sp^2c COC. This was consistent with the simulated mass (m/z 1007.2894) for the molecular formula $[C_{72}H_{36}N_6 + Na]^+$ (Fig. 1D and Fig. S8 in Supporting information). The chemical structure of the sp^2c COCs was also confirmed through Fourier transform infrared (FT-IR) spectroscopy (Fig. 1C, Fig. S9 in Supporting information). A peak at 2219 cm^{-1} , corre-

sponding to the cyano groups, was observed. Additionally, signals at 1631 and 1603 cm^{-1} , which are attributed to the C–H stretching vibrations of C=CH, were detected, providing strong evidence for the formation of C=C bonds [2,19]. Considering that the C=C bond imparts high chemical stability to the sp^2c COC, we aimed to explore the photoelectric properties of this highly conjugated COC. To facilitate this comparison, we synthesized imine COC with the same skeleton via a Schiff base reaction (Scheme S2 in Supporting information) [20,21]. The successful synthesis of imine COC was confirmed through comprehensive characterization techniques, including nuclear magnetic resonance (NMR), HRMS, and FT-IR (Fig. 1C, Figs. S9-S11 in Supporting information).

The UV–visible and photoluminescent spectra revealed that sp^2c COC exhibited an absorption curve similar to that of imine COC, with both showing absorption at 409 nm. However, the absorption and emission peaks of sp^2c COC were relatively broad, likely due to π - π stacking associated with its high degree of conjugation, which aligns with the observed poor solubility of sp^2c COC in dimethyl sulfoxide (DMSO) [13,22]. Nevertheless, the photoluminescent spectrum of sp^2c COC displayed a maximum at 518 nm, indicating a 29 nm red shift compared to that of imine COC (Figs. S12-S14 in Supporting information). The significant fluorescent properties and large Stokes shift (109 nm) for sp^2c COC further indicated that (a) the lowest energy transition is dominated by the anthracene arms, and (b) the C=C bonds can better transmit conjugation along the COC backbone, enhancing electron delocalization. This improved delocalization, in turn, can lead to more stable excited states and reduce energy loss during the emission process, resulting in sharper emission features [15,23,24].

The UV–visible diffuse reflectance spectra (DRS) for sp^2c COC and imine COC, illustrated in Fig. 2A, revealed that both COCs demonstrated strong absorption in the ultraviolet and visible light regions, with their absorption intensity increasing upon exposure to light. Tauc plot analysis revealed that both sp^2c COC and imine COC had a band gap of 2.36 eV, highlighting their potential as visible light-responsive photocatalysts (Fig. 2B). Notably, sp^2c COC showed an absorption onset at 1500 nm, significantly higher than that of imine COC at 800 nm. This suggested that the introduction of C=C bonds enhanced the light absorption range and caused a pronounced red shift in the absorption edge, allowing sp^2c COC to utilize a broader spectrum of light [14,25].

To gain a deeper understanding of the photophysical properties and electrochemical performance of sp^2c COC, we carried out a thorough evaluation using an electrochemical workstation, which included techniques such as cyclic voltammetry (CV), electrochemical impedance spectroscopy (EIS) Nyquist plots, and Mott–Schottky (M–S) analysis. The CV curve shows that the initial oxidation potential (0.38 V) and initial reduction potential (−0.69 V) of sp^2c COC are both lower than those of the imine COC (with initial oxidation and reduction potentials of 0.58 V and −0.83 V, respectively), indicating relatively stronger redox capabilities. (Fig. 2C). This suggested that sp^2c COC could be more effective in facilitating redox reactions, and its band structure promoted electron transfer and reactant transformation [26]. As illustrated in Fig. 2D, the EIS Nyquist plots showed that the arc radius of sp^2c COC was smaller than that of imine COC. This suggested that sp^2c COC exhibited lower electrochemical impedance and reduced charge transfer resistance, highlighting its excellent electrochemical activity and charge transfer properties. Subsequently, Mott–Schottky (M–S) analysis was employed to further determine the conduction band (E_{CB}) and valence band (E_{VB}) values, clarifying their energy band structure in conjunction with the measured optical band gap (Fig. 2E, Fig. S15 in Supporting information). Both sp^2c COC and imine COC exhibited typical n-type semiconductor characteristics, with flat band potentials determined to be −1.62 V and −1.92 V, respectively. Combining the Tauc plots, the E_{CB} positions of sp^2c COC

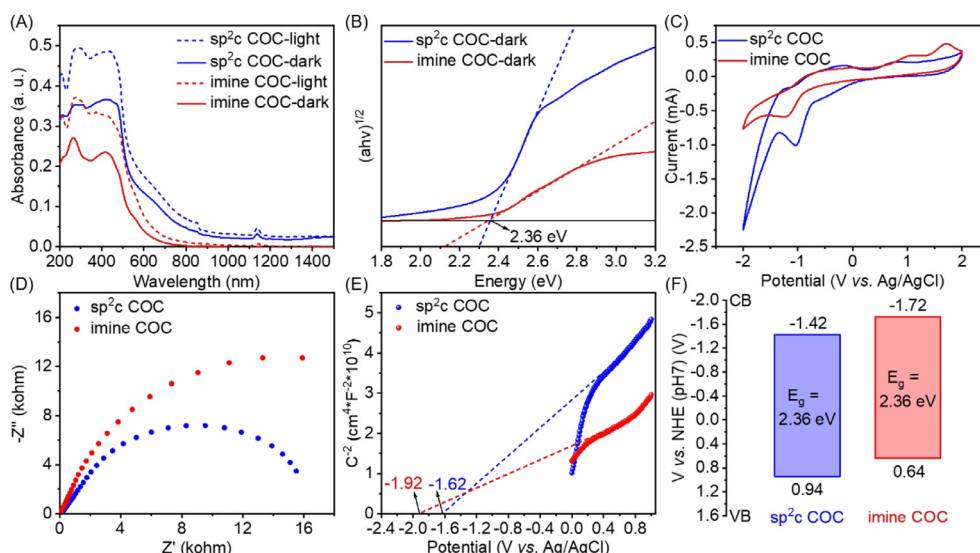


Fig. 2. Optoelectrical properties of sp^2c COC and imine COC. (A) UV-vis DRS of sp^2c COC and imine COC powders under dark and light conditions. (B) Tauc plots of sp^2c COC and imine COC. (C) CV curves of sp^2c COC and imine COC films. (D) EIS Nyquist plots of sp^2c COC and imine COC. (E) M-S plots of sp^2c COC and imine COC. (F) Band structures of sp^2c COC and imine COC.

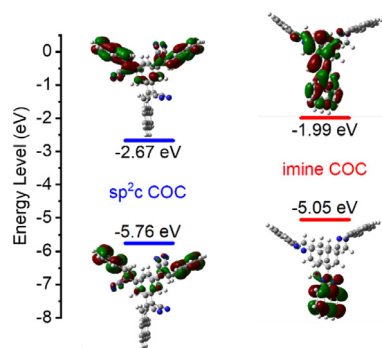


Fig. 3. Energy diagrams and visual representations of the frontier molecular orbitals of sp^2c COC and imine COC.

and imine COC were determined to be -1.42 V and -1.72 V, respectively, while the E_{VB} positions were 0.94 V and 0.64 V (vs. NHE at pH 7) (Fig. 2F). Given that the E_{CB} level of COCs was more negative than the reduction potential of O_2 to the superoxide radical anion ($E(O_2/O_2^{\cdot-}) = -0.33$ V vs. NHE), the photocatalytic generation of $O_2^{\cdot-}$ is theoretically achievable [27–29].

Subsequently, geometric optimization and determination of the molecular orbital energy levels of sp^2c COC and imine COC were performed using time-dependent density functional theory (TD-DFT) with the B3LYP/6–31G(d,p) basis set. The estimated highest occupied molecular orbital (HOMO) of sp^2c COC was -5.76 eV, and its lowest unoccupied molecular orbital (LUMO) was -2.67 eV, both lower than those of imine COC (-5.05 eV and -1.99 eV), aligning with the band structures of COCs (Fig. 3, Fig. S16 in Supporting information). This indicated that sp^2c COC may offer better electron stability in the excited state [15,30,31]. Combining the results of the optical band gap and CV curves, the analysis showed that sp^2c COC benefitted from its excellent light absorption capacity, which facilitated the separation of electron-hole pairs upon photoexcitation. Additionally, sp^2c COC exhibited a more favorable energy distribution for reactions after photoexcitation, promoting the rapid transfer of excited electrons to the reaction sites. This effectively converted light energy into chemical energy, thereby enhancing photocatalytic efficiency. In sp^2c COC, it was noteworthy that the HOMO and LUMO distributions were consistent, located on the

two anthracene arms and adjacent cyanoethylene bonds. Furthermore, the energy levels of HOMO and HOMO-1, as well as LUMO and LUMO+1, were identical—an observation not seen in imine COC. This highlighted that the excellent stability and reactivity of sp^2c COC stem from its highly symmetrical molecular structure, correlating with its elevated conjugation degree [5,14,22,24,32,33]. The presence of cyanoethylene bonds enhances the molecular orbital symmetry and energy level similarity between COCs within the same skeletons, resulting in well-coordinated electronic density and orbital distribution within the cage molecule. This facilitates the separation and migration of electron-hole pairs, thereby improving photocatalytic performance [34].

Tests such as photocurrent (i -T), electron paramagnetic resonance (EPR) spectroscopy, and transient fluorescence lifetime were used to verify the photoresponsiveness and charge carrier properties of sp^2c COC and imine COC. The i -T curves clearly demonstrated the photo-responsiveness of both COCs, with the positive transient currents reinforcing their n-type semiconductor characteristics (Fig. 4A). The sp^2c COC exhibited notable photo-responsiveness, showing a minimum dark current density of about $9.13 \mu A/cm^2$ and a maximum photo current density of approximately $11.99 \mu A/cm^2$. In comparison, the imine COC had a minimum dark current density of around $5.15 \mu A/cm^2$ and a maximum photo current density of about $5.85 \mu A/cm^2$. These findings aligned with the trends observed in the DRS and EIS data. The conjugated skeleton granted electron transport properties to both COC types. Especially for sp^2c COC, the presence of C=C bonds promoted the generation of photogenerated charge carriers, reduced recombination rates, and improved charge transfer, ultimately enhancing photocatalytic performance. The photoresponsive EPR further validated and explained the differences in photo-responsiveness (Fig. 4B). Under non-irradiated conditions, both sp^2c COC and imine COC exhibited a distinct free radical signal at $g = 2.003$ [13,35]. The EPR signal of sp^2c COC was notably stronger than that of imine COC. After excitation under the same illumination conditions, the EPR signal of sp^2c COC significantly increased, whereas the signal for imine COC remained virtually unchanged. The photoactivity of the anthracene moiety and the conjugated skeletons enabled both sp^2c COC and imine COC to possess intrinsic electron-hole pairs that can separate and facilitate charge carrier migration. The C=C bonds effectively modulated the energy distribution of the excited states, allowing the sp^2c COC's band structure and high stability to pro-

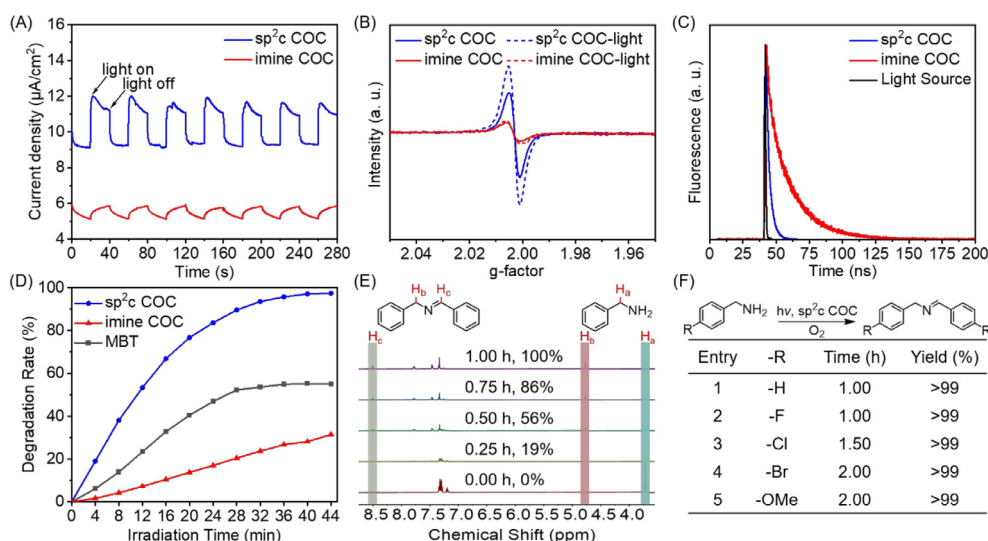


Fig. 4. The photocatalytic performance of sp^2c COC and imine COC. (A) *i*-*T* plots of two COCs. (B) The EPR spectra of two COCs under dark and light irradiation conditions. (C) Transient fluorescence spectra of sp^2c COC and imine COC. (D) Degradation of MBT under light irradiation with and without sp^2c COC or imine COC as photocatalyst. (E) Photocatalytic oxidation of benzylamine to *N*-benzylidene benzylamine using sp^2c COC as photocatalysis under irradiation for different time. (F) Conversion of the photocatalytic oxidation of different amine to imine by sp^2c COC photocatalysis.

mote efficient generation and migration of photogenerated charge carriers within its molecular skeleton. While imine COC showed a weaker photoelectric response, its higher internal electrochemical impedance hindered electron transfer pathways, preventing these radicals from effectively contributing to photoelectric current generation. The transient fluorescence lifetime results showed that the average fluorescence lifetime of sp^2c COC is 2.86 ns, significantly shorter than imine COC's 17.92 ns (Fig. 4C). This confirmed that under light excitation, sp^2c COC efficiently generated photogenerated charge carriers, enabling their rapid migration to reaction sites and converting light energy into chemical energy to enhance photocatalytic reactions [15,19,35]. Additionally, in the imine COC, the imine nitrogen weakened the electron delocalization of the C=N bond, resulting in photogenerated charge carriers that are unable to effectively migrate to the reaction sites, thereby hindering the reaction [14,15,19,26]. Overall, rational energy band structure and semiconductor characteristics of sp^2c COC provided it with the potential to act as a metal-free catalyst. While imine COC exhibits semiconductor characteristics, imine nitrogen as a vulnerable site in the COC skeleton, significantly restricts their application range.

Preliminarily, we chose the classic organic dye photodegradation reaction to verify the photocatalytic activity of the two COCs. Considering the low overlap of light absorption with COCs, we conducted tests using methylene blue trihydrate (MBT) as a representative [19]. In the absence of any COC as a photocatalyst, MBT reached its maximum degradation rate (55%) after 36 min of light exposure. When sp^2c COC was added as a photocatalyst, the degradation rate of MBT nearly doubled, achieving almost complete degradation (97%) within 40 min. In contrast, the presence of imine COC hindered the photodegradation of MBT, with only a 31% degradation rate achieved after 44 min of light exposure (Fig. 4D, Fig. S17 in Supporting information). This observed inhibition of MBT degradation can be partly attributed to imine COC's absorption of visible light, which leads to its photodegradation. This, in turn, reduces MBT's ability to absorb visible light, thereby inhibiting its own photocatalytic degradation process (Fig. S18 in Supporting information). These findings were consistent with the previously analyzed photophysical properties and photoresponsiveness.

Based on the aforementioned research, we chose challenging and environmentally friendly photocatalytic aerobic oxidation ex-

periments to further validate the photocatalytic performance of sp^2c COC (Figs. 4E and F, Fig. S19-S29 in Supporting information). The experiment began with the selection of the conversion of benzylamine to *N*-benzylidene benzylamine as the model reaction [14,26,27]. In open-air and irradiation conditions, the conversion rate of benzylamine increased progressively with longer irradiation time. Within 1 h, benzylamine was nearly fully converted to *N*-benzylidene benzylamine. In the absence of any special treatments or activation conditions, the sp^2c COC still exhibited high catalytic activity. After adding excess benzylamine and repeating the experiment three times, it consistently achieves a high photocatalytic conversion efficiency (higher than 99%), which also demonstrates its notable photostability.

Following this, we performed photocatalytic oxidation reactions on benzylamine substrates with various substituents under identical conditions. The consistently high conversion rates further demonstrated the broad applicability of sp^2c COC for the photocatalytic oxidation of benzylamine to imines. Future, we used EPR test to confirm the existence of $O_2^{\cdot-}$ via the scavengers of 5-dimethyl-1-pyrroline (DMPO) under visible light illumination, which indicates that sp^2c COC has a certain ability to generate reactive oxygen species (ROS), playing a vital role in converting amine into imine (Fig. S30 in Supporting information). This effectiveness can be attributed to the favorable band structure of sp^2c COC, its enhanced charge separation and migration capabilities, and reduced interfacial resistance, all of which have been validated through photocurrent response, EPR, and EIS measurements. The possible photocatalytic mechanism analysis reveals that sp^2c COC undergo efficient generation of electron-hole pairs under photoexcitation. Primary photocatalytic pathways involve: (1) Direct redox mediation where these photon-generated carriers interact with dye molecules or benzylamine substrates, driving either molecular degradation or selective oxidation to imine derivatives; (2) Partial photogenerated electrons in the conduction band react with dissolved O_2 , yielding superoxide anion ($O_2^{\cdot-}$) that establish a synergistic effect on the overall photocatalytic process (Fig. S31 in Supporting information). We also estimated the thermal stability of sp^2c COC through thermogravimetric analysis (TGA), which reveals its excellent thermal stability, with 73% residual mass remaining after heating to 800 °C under N_2 (Fig. S32 in Supporting information). Meanwhile, the unchanged optical absorption peak

shape and intensity demonstrate that sp^2c COC maintains stability in boiling water as well as in corrosive solutions, including concentrated HCl, HNO_3 , H_2SO_4 and saturated NaOH. Additionally, the minimal weight loss observed before and after immersion further confirms the chemical stability of sp^2c COC under these conditions (Fig. S33 and Table S2 in Supporting information).

In conclusion, we have developed a novel fully conjugated anthracene-based COC via the Knoevenagel condensation of An-2CHO and BTN. The C=C bonds between An-2CHO and BTN monomers form a highly conjugated structure with excellent chemical stability. This sp^2c COC exhibits outstanding photoreponsive semiconductor properties, allowing efficient conduction of photogenerated carriers. It effectively drives the photocatalytic degradation of MBT and the conversion of amines to imines, showing superior efficiency and reusability compared to imine COC. This innovation broadens the potential applications of COCs in photocatalysis and provides a new avenue for research. We believe the design and functionalization of highly conjugated, sp^2 carbon-linked COCs offer a promising strategy for developing optically active materials.

Declaration of competing interest

The authors declare that they have no known competing financial interests or personal relationships that could have appeared to influence the work reported in this paper.

CRediT authorship contribution statement

Jiajia Li: Writing – original draft, Methodology, Investigation, Data curation. **Shan Shiang Hii:** Investigation, Data curation. **Xinyuan Zhu:** Resources. **Yanping Yang:** Supervision. **Youfu Wang:** Writing – review & editing, Supervision.

Acknowledgments

This work was supported by the Class III Peak Discipline of Shanghai-Materials Science and Engineering (High Energy Beam Intelligent Processing and Green Manufacturing), and Fundamental Research Funds for the Central Universities (Nos. YG2023QNA04 and YG2022QN027).

Supplementary materials

Supplementary material associated with this article can be found, in the online version, at doi:10.1016/j.ccllet.2025.111151.

References

- [1] J. Li, Y. Yang, J. Yang, et al., *Coord. Chem. Rev.* 523 (2025) 216260.
- [2] F. Qiu, X. Chen, W. Wang, K. Su, D. Yuan, *CCS Chem.* 6 (2024) 149–156.
- [3] Y. Ni, F. Gordillo-Gómez, M. Peña Alvarez, et al., *J. Am. Chem. Soc.* 142 (2020) 12730–12742.
- [4] D. Cui, F. Bai, L. Zhang, et al., *Angew. Chem. Int. Ed.* 63 (2024) e202319815.
- [5] K. Matsui, Y. Segawa, K. Itami, *J. Am. Chem. Soc.* 136 (2014) 16452–16458.
- [6] M. Servalli, N. Trapp, M. Wörle, *J. Org. Chem.* 81 (2016) 2572–2580.
- [7] X. Gu, T.Y. Gopalakrishna, H. Phan, *Angew. Chem. Int. Ed.* 56 (2017) 15383–15387.
- [8] S. Wu, Y. Ni, Y. Han, et al., *Angew. Chem. Int. Ed.* 61 (2022) e202115571.
- [9] S.J. Rowan, S.J. Cantrill, G.R.L. Cousins, J.K.M. Sanders, J.F. Stoddart, *Angew. Chem. Int. Ed.* 41 (2002) 898–952.
- [10] K.D. Okochi, G.S. Han, I.M. Aldridge, Y. Liu, W. Zhang, *Org. Lett.* 15 (2013) 4296–4299.
- [11] Q. Wang, C. Yu, C. Zhang, et al., *Chem. Sci.* 7 (2016) 3370–3376.
- [12] J. You, Y. Zhao, L. Wang, W. Bao, *J. Clean. Prod.* 291 (2021) 125822.
- [13] E. Jin, M. Asada, Q. Xu, et al., *Science* 357 (2017) 673–676.
- [14] R. Chen, J. Shi, Y. Ma, et al., *Angew. Chem. Int. Ed.* 58 (2019) 6430–6434.
- [15] J. Cheng, Y. Wu, W. Zhang, et al., *Adv. Mater.* 36 (2024) 2305313.
- [16] D. Becker, B.P. Biswal, P. Kalefczuk, et al., *Chem. Eur. J.* 25 (2019) 6562–6568.
- [17] A.N. Kumar, R. Naik, V. Revathi, et al., *Appl. Surf. Sci. Adv.* 14 (2023) 100392.
- [18] T. Zhou, L. Wang, X. Huang, et al., *Nat. Commun.* 12 (2021) 3934.
- [19] Y. Yang, H. Niu, L. Xu, H. Zhang, Y. Gai, *Appl. Catal. B: Environ.* 265 (2020) 118799.
- [20] G.H. Ning, P. Cui, I.V. Sazanovich, et al., *Chem* 7 (2021) 3157–3170.
- [21] D. Wang, L. Zhang, Y. Zhao, *J. Org. Chem.* 87 (2022) 2767–2772.
- [22] X. Li, *Mater. Chem. Front.* 5 (2021) 2931–2949.
- [23] S. Ghosh, Y. Tsutsui, K. Suzuki, et al., *Mol. Syst. Des. Eng.* 4 (2019) 325–331.
- [24] Z. Zhang, Y. Zhu, X. Chen, et al., *Adv. Mater.* 31 (2019) 1806626.
- [25] H. Hao, F. Zhang, X. Dong, X. Lang, *Appl. Catal. B: Environ.* 299 (2021) 120691.
- [26] J.L. Shi, R. Chen, H. Hao, C. Wang, X. Lang, *Angew. Chem. Int. Ed.* 59 (2020) 9088–9093.
- [27] S.D. Wang, C.L. Lai, Y.X. Zhang, et al., *J. Mater. Chem. A* 10 (2022) 20975–20983.
- [28] G. Che, W. Yang, C. Wang, *Inorg. Chem.* 61 (2022) 12301–12307.
- [29] Y. Yang, J. Kang, Y. Li, et al., *New J. Chem.* 46 (2022) 21605–21614.
- [30] Z. Chen, J. Wang, M. Hao, et al., *Nat. Commun.* 14 (2023) 1106.
- [31] Y.Z. Cheng, W. Ji, X. Wu, et al., *Appl. Catal. B: Environ.* 306 (2022) 121110.
- [32] K. Matsui, Y. Segawa, T. Namikawa, K. Kamada, K. Itami, *Chem. Sci.* 4 (2013) 84–88.
- [33] T. He, K. Geng, D. Jiang, *Trends Chem.* 3 (2021) 431–444.
- [34] Y. Chen, D. Jiang, *Acc. Chem. Res.* 57 (2024) 3182–3193.
- [35] J. Chen, K. Zhang, X. Zhang, et al., *Chem. Eur. J.* 30 (2024) e202303725.